ISSN 0030-400X, Optics and Spectroscopy, 2010, Vol. 108, No. 3, pp. 417–424. © Pleiades Publishing, Ltd., 2010.

SINGLE-PHOTON SOURCES

Room-Temperature Single Photon Sources with Definite Circular and Linear Polarizations[1]

S. G. Lukishova, L. J. Bissell, C. R. Stroud, Jr., and R. W. Boyd

The Institute of Optics University of Rochester, Rochester NY, 14627 USA

e-mail: sluk@lle.rochester.edu

Received August 3, 2009

Abstract—We report experimental results of two room-temperature single photon sources with definite polarization based on emitters embedded in either cholesteric or nematic liquid crystal hosts. In the first case, a cholesteric 1-D photonic bandgap microcavity provides circular polarization of definite handedness of single photons from single colloidal semiconductor quantum dots (nanocrystals). In these experiments, the spectral position of the quantum dot fluorescence maximum is at the bandedge of a photonic bandgap structure. The host does not destroy fluorescence antibunching of single emitters. In the second case, photons with definite linear polarization are obtained from single dye molecules doped in a planar-aligned nematic liquid crystal host. The combination of sources with definite linear and circular polarization states of single photons can be used in a practical implementation of the BB84 quantum key distribution protocol.

DOI: 10.1134/S0030400X10030161

1. INTRODUCTION

The development of on-demand efficient single-photon sources (SPSs) with photons exhibiting antibunching has recently been of significant interest for their applications in quantum cryptography [1]. Weak attenuated light sources are not satisfactory because in order to attenuate the source sufficiently so that two simultaneous photons are very unlikely the probability of no photons at all becomes large. In the BB84 quantum key distribution protocol Alice (transmitter) and Bob (receiver) employ the linear and circular polarization states of single photons. The linear and circular bases are used to provide two different quantum level representations of zero and one [2, 3]. So a desirable feature for a SPS is definite photon polarization, since if the photon has unknown polarization, then filtering it through a polarizer to produce the desired polarization for quantum key distribution will reduce twice the SPS efficiency.

In this paper, experimental results of room-temperature, robust SPSs on demand with definite polarization using single-emitter fluorescence in different liquid crystal (LC) hosts are discussed [4–8]. A desirable polarization state (either circular with definite handedness or linear with definite direction) of a fluorescence of the emitter in a LC host can be produced either by providing a chiral microcavity environment of cholesteric LC (CLC) or by aligning emitters' dipole moments in a definite direction in nematic LC. SPSs based on single emitters in LCs are the room temperature alternatives to cryogenic SPSs based on semiconductor heterostructured quantum dots in microcavities prepared by molecular beam epitaxy (MBE) (see reviews [9, 10]). Definite linear polarization from heterostructured quantum dots both in elliptical pillar microcavities [11–13] and in 2-D photonic crystal [14, 15] was reported for the resonance wavelength at cryogenic temperatures. In difference to expensive MBE, well-developed LC display technology of preparation of planar-aligned 1-D photonic bandgap CLC layers or planar-aligned nematic LC layers is easy and fast. Different types of single emitters can be easily dissolved or dispersed both in monomeric (fluid-like) or oligomeric (solid) LCs. In addition to emitter alignment and self-assembled structures with photonic bandgap properties, LC hosts with special treatment (oxygen depletion) can protect the emitters from bleaching. In paper [4], we reported on a significant diminishing of dye bleaching by saturation of LC with helium. In that work molecules did not bleach for periods of more than one hour under continuous wave (cw) excitation [4]. Another remarkable advantage of LC, e.g., changing its properties with temperature or by external field variation, can provide SPS tunability.

The structure of this paper is as follows. Section 2 describes the results on antibunching and circular polarized fluorescence with desired handedness of colloidal semiconductor quantum dots (QD) embedded into planar-aligned CLC monomeric host. Section 3 is devoted to linearly polarized fluorescence with definite polarization state from single dye molecules aligned in a glassy nematic LC oligomer. Section 4 concludes the paper.

[1] The article is published in the original.

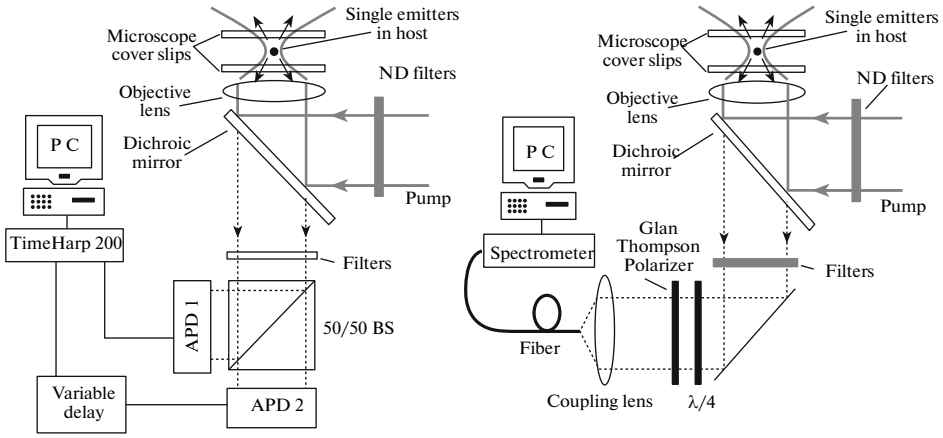

Fig. 1. Schematics of experimental setup for fluorescence imaging and antibunching measurements (left); spectral and polarization measurements (right). We used the following abbreviations: neutral density (ND), single-photon counting avalanche photodiode module (APD), beamsplitter (BS).

2. SINGLE-PHOTON SOURCE WITH CIRCULARLY POLARIZED PHOTONS

The first SPS is based on the single colloidal CdSe (fluorescence wavelength $\lambda_0 \sim 580$ nm) and CdSeTe ($\lambda_0 \sim 700$ nm) QDs suspended in a CLC hosts self-assembled in a chiral photonic bandgap structures. This structure can provide not only spontaneous emission enhancement and a diminishing of the fluorescence lifetime, but also circular polarization of definite handedness even for emitters without a dipole moment. In addition, because the refractive index n varies gradually in chiral structures rather than abruptly, there are no losses into the waveguide modes, which arise from total internal reflection at the border between two consecutive layers with different n. We report here for the first time fluorescence antibunching of a QD doped in a LC. Earlier we reported fluorescence antibunching of dye embedded in LC host [4]. Room-temperature SPSs based on colloidal QD fluorescence are very promising because of higher QD photostability at room temperature than that of conventional dyes, and relatively high quantum yield (up to ~100%) [16]. Electrically driven light emission from a single colloidal QD at room temperature was obtained, opening up the possibility for electrical pumping of a SPS on demand, based on colloidal QDs [17]. Nonblinking, long-lasting colloidal QDs were reported recently [18].

2.1. Experimental Setup for Antibunching and Circular Polarization Measurements

The experimental setup consists of a home-built confocal fluorescence microscope based on a Nikon TE2000-U inverted microscope with several output ports. Figure 1 shows the abbreviated schematics of our experiment for fluorescence imaging and antibunching measurements (left) and polarization and spectral measurement (right).

We excite our samples with 76 MHz repetition-rate, 6 ps pulse duration, 532 nm light from a Lynx mode-locked laser (Time-Bandwidth Products Inc.). To obtain a diffraction-limited spot on the sample, the excitation beam is expanded and collimated by a telescopic system with a spatial filter. The samples are placed in the focal plane of a 1.3-numerical aperture, oil-immersion microscope objective used in confocal reflection mode. In focus, the intensities used are of the order of several kW/cm^2. Residual transmitted excitation light is removed by a dichroic mirror and a combination of two interference filters yielding a combined rejection of nine orders of magnitude at 532 nm. The sample's holder is attached to a piezoelectric, XY translation stage providing a raster scan of the sample through an area up to 50 μm × 50 μm.

The following diagnostics are placed in the separate output ports:

(1) A Hanbury Brown Twiss arrangement consisting of a 50/50 beamsplitter and two cooled, Si single photon counting avalanche photodiode modules (APDs) SPCM AQR-14 (Perkin Elmer). The time interval between two consecutively detected photons in separate arms is measured by a TimeHarp 200 time correlated single-photon counting card using a conventional start-stop protocol.

(2) Electron multiplying, cooled CCD-camera iXon DV 887 ECS-BV (Andor Technologies).

(3) Fiber-optical spectrometer (Ocean Optics). The method of defining the dissymmetry of circular polarization is described in [19]. For circular-polarization measurements both an achromatic quarter waveplate and a Glan Thompson linear polarizer on rotating mounts are placed in the spectrometer port in front of the spectrometer. An area with several single

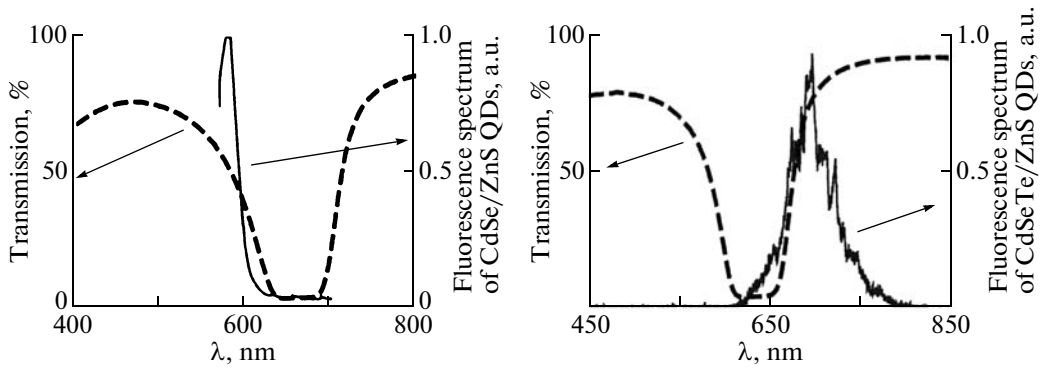

Fig. 2. Selective transmission of two monomeric chiral photonic bandgap CLC hosts for right-handed circular polarized light and the fluorescence spectrum of the CdSe (left) and CdSeTe (right) quantum dots.

QDs is selected by an EM-CCD camera in a wide-field mode and/or by APD-detectors with a raster-scan of the sample in a confocal mode. It is imaged to the spectrometer input fiber. The spectra are recorded with a 6-s accumulation time with background subtraction.

CdSe/ZnS core/shell QDs were synthesized by T. Krauss' group (University of Rochester) according to published methods [20, 21]. CdSeTe QDs were obtained commercially from Invitrogen.

2.2. Chiral Microcavities Made of Cholesteric Liquid Crystals Doped with Single Colloidal Quantum Dots: Preparation and Characterization

In a planar-aligned CLC, the rod-shaped anisotropic molecules with small chiral "tails" form a periodic helical structure with pitch p [22]. For sufficiently thick CLC layers, the reflectance of normally incident, circularly polarized light, with the same handedness as the CLC structure, is nearly 100% within a band centered at $\lambda_c = n_{av}p$. The bandwidth is approximately $\Delta\lambda = \lambda_c\Delta n/n_{av}$, where n_{av} the average of the ordinary n_o and extraordinary n_e refractive indices of the medium: $n_{av} = (n_o + n_e)/2$, and $\Delta n = n_e - n_o$. This periodic structure can also be viewed as a 1-D photonic crystal, with a bandgap within which propagation of light is forbidden. For emitters located within this structure, the spontaneous emission rate is suppressed within the spectral stopband and enhanced near the *band edge* [23, 24]. Both the literature [24] and our lasing experiments [25] in dye-doped CLC structures with high dopant concentration confirmed that the best condition for coupling is when the dopant fluorescence maximum is at a band edge of the CLC selective transmission curve.

For sample preparation we use monomeric mixtures of low-molecular-weight E7 nematic-LC blend with a chiral additive CB15. E7 and CB15 are fluids at room temperature. Both materials were supplied by EM Industries. We filtered E7 and CB15 to remove fluorescent contaminants.

For development of CLC hosts which form a chiral photonic bandgap tuned to the QD fluorescence band, two main aspects are important: (1) properly choosing the concentration of different LC components and (2) providing planar alignment of the CLC. For the monomeric mixtures, the stopband position λ_c of the photonic bandgap is defined roughly by $C = n_{av}/(\lambda_c \times \mathrm{HTP})$, where C is the weight concentration of CB15 in the CB15/E7 mixture, $n_{av} \sim 1.6$ for this mixture, and HTP ~ 7.3 μm^{-1} is the helical twisting power of the chiral additive in nematic LC. The actual stopband position relative to the fluorescence maximum of the QD is defined empirically by obtaining selective transmission curves of different samples using a spectrophotometer with a thin film linear polarizer and an achromatic quarter waveplate.

After monomeric CLC preparation, a QD solution of ~nM concentration is mixed with monomeric CLC and solvent is evaporated. After that, monomeric CLC doped with QDs is placed between two cover glass slips and planar aligned through unidirectional mechanical motion between the two slides. For further details of CLC doping and sample preparation see [5].

By properly choosing the concentration of different LC monomers and providing planar alignment of the LCs, we developed CLC chiral 1-D photonic bandgap structures with different stopband positions doped with single QDs (CdSe and/or CdSeTe). Increasing the concentration of a component with higher HTP changes the position of the stopband in the direction of shorter wavelengths. The error in defining weight concentrations (~±5%) can smear this effect for mixtures with similar concentrations. The stopband positions are tuned to the QD fluorescence bands (Fig. 2).

Figure 2 shows selective transmission curves of two monomeric 1-D chiral photonic bandgap structures with 36.6% (left) and 36% (right) weight concentra-

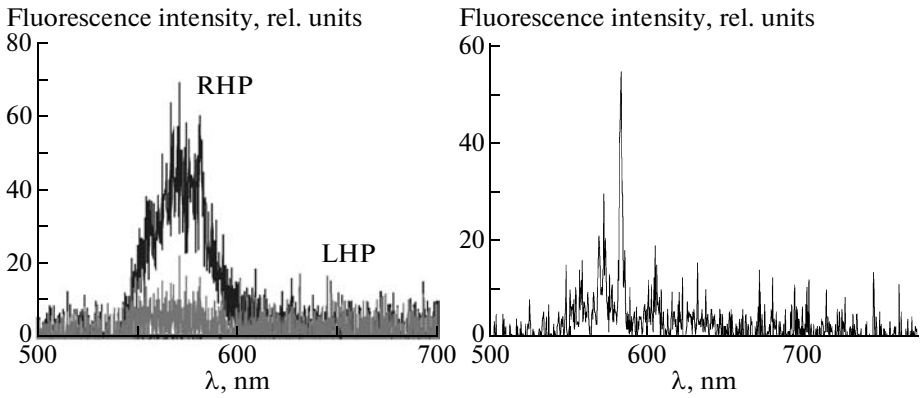

Fig. 3. Fluorescence spectrum of: CdSe QDs in the monomeric planar-aligned CLC host (selective transmission shown in Fig. 2, left) for two different circular polarizations of single photons (RHP—right handed, LHP—left handed)—left. The same monomeric CLC host without QDs—right.

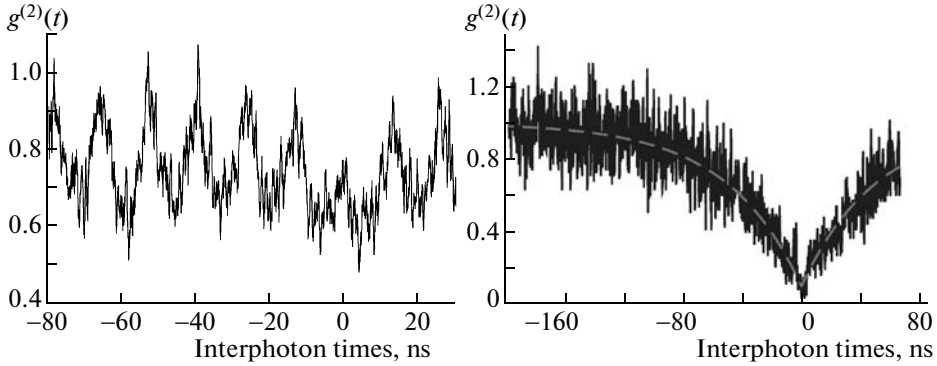

Fig. 4. Histograms of coincidence counts of single-QD fluorescence in a CLC host under pulsed excitation. The dip at zero interphoton time indicates antibunching. Left: for CdSe QD of Fig. 2, left with λ_0 within the liquid crystal background; right: for the CdSeTe QD of Fig. 2, right with λ_0 outside the liquid crystal background.

tions of chiral additive CB15 in E7/CB15 mixtures. It also shows the fluorescence spectra of the CdSe (left) and CdSeTe (right) QDs with the centers of the fluorescence peaks near 580 and 700 nm.

2.3. Circular Polarized Fluorescence and Antibunching in Chiral Cholesteric Liquid Crystal Microcavity

Figure 3 (left) shows emission spectra for CdSe/ZnS QDs in a chiral CLC microcavity for right-handed (black line) and left-handed circular polarizations (gray line). The degree of circular polarization is measured by the dissymmetry factor g_e [26]:

$$g_e = 2(I_L - I_R)/(I_L + I_R), \quad (1)$$

where I_L and I_R are the intensities of left-handed and right-handed circular polarizations. At 580 nm, $g_e = -1.6$. For unpolarized light $g_e = 0$. Using another type of CLC, e.g., Wacker CLC oligomers [5], left-handed circular polarization of single photons can be obtained.

The fluorescence spectrum of the same CLC microcavity without QDs is depicted in Fig. 3, right. The nature of the spectral peaks which were observed in the CLC cavity without QDs is unclear. It is not a microcavity effect, because we observed the same features from unaligned CLC without a microcavity. It can be attributed to some impurities which we did not remove during the LC purification procedure.

We also illuminated a single CdSe QD in the CLC host and measured the fluoresced photon statistics under saturation conditions. Figure 4, left presents the $g^{(2)}(t)$ histogram at different interphoton times t.

One sees that the peak at zero interphoton time is clearly smaller than any of the other peaks, which shows an antibunching property [$g^{(2)}(0) = 0.76 \pm 0.04$]. This antibunching histogram can be improved by using QDs which fluoresce outside the fluorescence spectrum of the CLC shown in Fig. 2, right. At wavelengths

larger than ~700 nm, no host background is observed. For a CdSeTe colloidal QD with a 700 nm fluorescence maximum (outside of the background spectrum of CLC with the stopband shown in Fig. 2, right), we obtained antibunching under saturation conditions with $g^{(2)}(0) = 0.11 \pm 0.06$ (Fig. 4, right). It shows that excluding the CLC background helps to obtain better antibunching. This QD has a fluorescence lifetime larger than the pulse repetition period of 13.2 ns, so we can not observe fluorescence excited by the separate laser pulses.

Estimation of the efficiency P of polarized single-photon emission into the collecting objective showed $P \sim 15\%$ with the second-order correlation function $g^{(2)}(0) = 0.11 \pm 0.06$, measured from the antibunching histogram of Fig. 4, right using 257 nW excitation power. We defined P from the following equation:

$$[1 - g^{(2)}(0)]N_{\text{out}} = N_{\text{incQD}}\alpha\beta G Q_{\text{APD}} P, \qquad (2)$$

where $N_{\text{out}} = 2.86 \times 10^4$ counts/s is the measured photon count rate by the APDs and $N_{\text{incQD}} = N_{\text{inc}}\sigma_{\text{absQD}} = (I/h\nu)\sigma_{\text{absQD}} = 2.35 \times 10^6$ photons/s is the number of photons incident on the quantum dot per second. Here, I is the measured incident intensity in the focal area of the sample ($I = 110$ W/cm^2), $h\nu = 3.73 \times 10^{-19}$ J for 532-nm light, and $\sigma_{\text{absQD}} = 8.0 \times 10^{-15}$ cm^2 is the absorption cross-section of the quantum dot at 532 nm taken from the measurements of Leatherdale et al. [27] as well as calculated from vendor's measurements of extinction coefficient [28].

Other parameters of Eq. (2) are as follows: $\alpha = 0.62$ is the measured transmission of all interference filters in front of the APDs, $\beta = 0.29$ is the measured transmission and collection of fluorescent light by the objective, microscope optics, and imaging lenses, $G = 0.59$ is the measured CdSeTe/ZnS QD quantum yield [28], and $Q_{\text{APD}} = 0.66$ is the quantum efficiency of the APD at 700 nm provided by the vendor.

The value of P characterizes the cavity (collection efficiency from the source into the collecting objective), and the value of PG characterizes both the cavity and the fluorescent emitter together. In our measurements for on-demand polarized single-photon source, $P \sim 15\%$, and $PG \sim 9\%$.

3. SINGLE PHOTON SOURCE WITH LINEARLY POLARIZED PHOTONS

The second SPS is based on a single dye molecule fluorescence suspended in LCs [4–7]. The results on dye fluorescence antibunching in LC host are reported in our papers [4–6]. We will describe here the results on definite linear polarization of fluorescence of single $DiIC_{18}(3)$ dye molecules in a planar-aligned glassy nematic LC host which is solid at room temperature.

3.1. Experimental Setup for Linear Polarization Measurements of Single Dye Molecules

Single-molecule fluorescence microscopy for this SPS is carried out on a Witec alpha-SNOM microscope in confocal mode. See details of the setup in [6]. The cw, spatially filtered, 532 nm, diode-pumped Nd:YAG laser output excites single molecules. To obtain a diffraction limited spot on the sample, the excitation beam is expanded and collimated by the optical system of Witec microscope [29]. In-focus, the intensities used were of the order of several kW/cm^2. The dye-doped nematic LC sample is placed in the focal plane of a 1.4-numerical aperture, oil-immersion microscope objective used in confocal transmission mode. Light emitted by the sample is collected by a confocal setup using a second oil-immersion objective with a 1.25-numerical aperture, an imaging lens with a focal length 12.5 cm and an aperture in a form of optical fiber. For polarized fluorescence measurements, we place inside the Witec microscope both a 50/50 polarizing beamsplitter cube and the second arm of the confocal detection. The confocal microscope apertures were 100 μm core optical fibers placed in each arm of the beamsplitter's output. Residual transmitted excitation light was removed by filters yielding a combined rejection of better than seven orders of magnitude at 532 nm. Photons in the two arms were detected by SPCM AQR-14 APD modules.

3.2. Sample Preparation from Planar-Aligned Glassy Nematic LC Oligomer Doped with Single Dye Molecules

For these experiments we use $DiIC_{18}(3)$ dye (DiI dye) from Molecular Probes in planar-aligned, glassy nematic liquid crystal host which is solid at room temperature. The dye molecular structure is presented in Fig. 5a. An oligomer host material was synthesized by S.H. Chen's group (University of Rochester) [30]. The nematic LC state of this material, which exists at elevated temperatures, is preserved at room temperature by slowly cooling to room temperature the LC to the solid glassy state with frozen nematic order [30]. An oligomer solution with a 1% concentration by weight in chloroform with 10 nM concentration of the dye in chloroform was prepared. We prepared ~100 nm thick film of this planar-aligned glassy, nematic LC guest-host system by several procedures including spin-coating on a cover glass slip with a photoaligned polymer layer, heating and slowly cooling the sample [6].

3.3. Linearly Polarized Fluorescence from Single Dye Molecules

Figure 5b shows images of single-molecule fluorescence for components perpendicular (left) and parallel (right) to the alignment direction, under 532-nm, cw-excitation. These two polarization components in the plane of the sample have been separated with a polarizing beamsplitter cube [6]. Figure 5b clearly

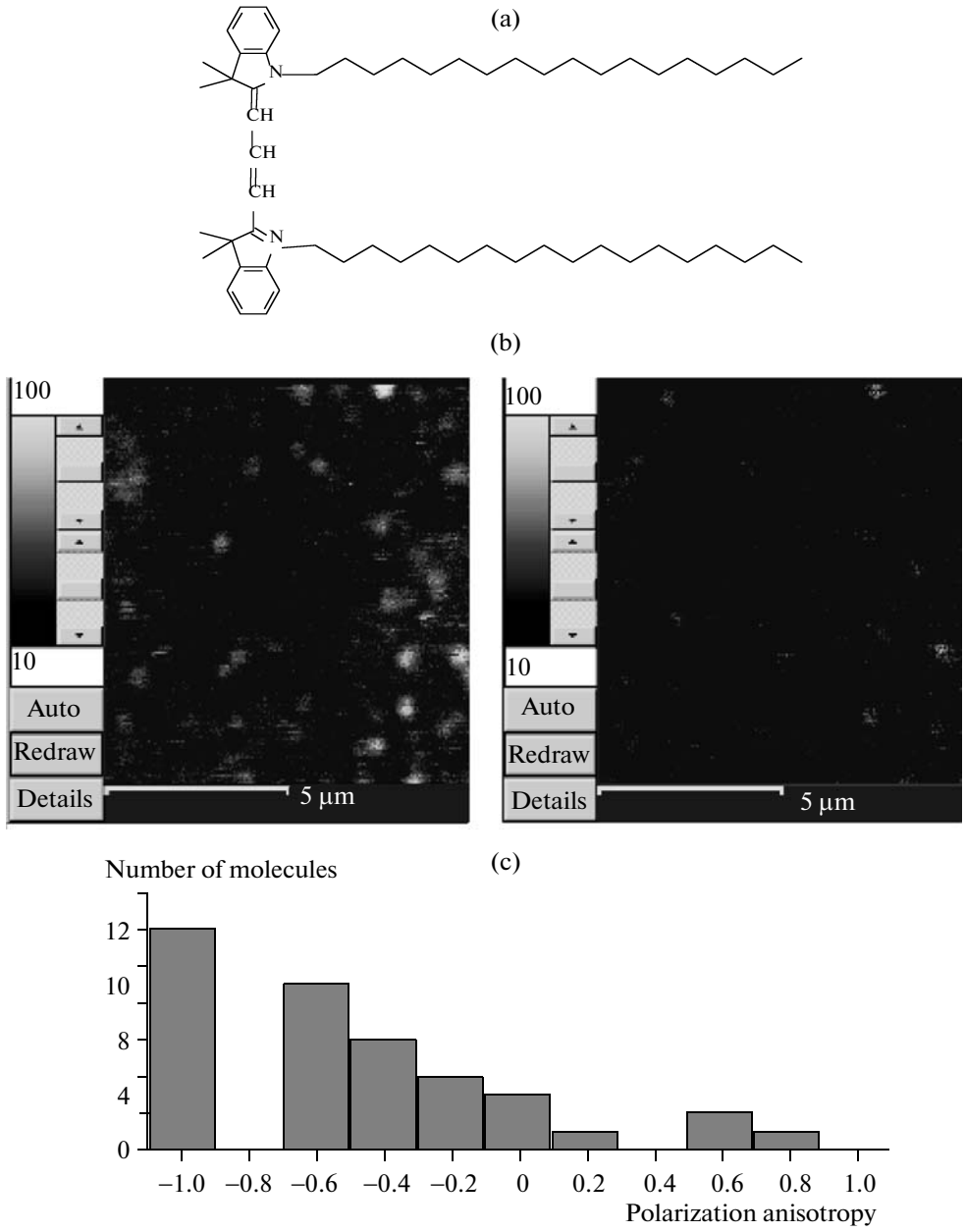

Fig. 5. (a) Molecular structure of $DiIC_{18}(3)$ dye. (b) Confocal fluorescence microscopy images of $DiIC_{18}(3)$ single-molecule fluorescence in planar-aligned glassy nematic liquid-crystal host (10 × 10 μm scan): left—polarization perpendicular to the alignment direction; right—parallel polarization. (c) The histogram of polarization anisotropy of 38 molecules of $DiIC_{18}(3)$ dye in planar-aligned glassy nematic liquid-crystal host. In difference with [31] with a symmetrical histogram for random orientation of $DiIC_{18}(3)$ dye molecular dipoles this histogram is asymmetrical.

shows that for this sample, the polarization direction of the fluorescence of single molecules is predominantly in the direction perpendicular to the alignment of LC molecules. It is important that the background level of left and right images of Fig. 5b is the same (~10 counts/pixel or ~640 counts/s). The single-molecule-fluorescence signal exceeds this background by up to 15 times.

The polarization anisotropy for a DiI dye is defined here as

$$\rho = (I_{par} - I_{perp})/(I_{par} + I_{perp}), \quad (3)$$

where I_{par} and I_{perp} are fluorescence intensities for polarization components parallel and perpendicular to the alignment direction [31]. Processing the images of Fig. 5b with background subtraction shows that

from a total of 38 molecules, 31 molecules have a negative value of ρ [a histogram of Fig. 5c]. The same sign of the polarization anisotropy [32] we obtained in spectrofluorimeter measurements for a sample with high (~0.5%) weight concentration of the same dye in a planar aligned glassy nematic LC layer with ~4.1 μm thickness [6]. This predominance of "perpendicular" polarization on Figs. 5b and 5c can be explained by DiI dye molecular structure (Fig. 5a). The two alkyl chains likely orient themselves parallel to the rod-like LC molecules, but the emitting/absorbing dipoles which are parallel to the bridge (perpendicular to alkyl chains) will be directed perpendicular to the LC alignment. DiI molecules orient in the same manner in cell membranes [33]. It should be noted that in [34] single terrylene dye molecules were uniaxially oriented in rubbed polyethylene although this paper did not provide the results on deterministically polarized fluorescence of single molecules.

Note that the images in Fig. 5b were taken by raster scanning the sample relative to the stationary, focused laser beam. The scan direction was from left to right and, line by line, from top to bottom. The size of the bright features is defined by the point-spread function of the focused laser beam. These images contain information not only about the spatial position of the fluorescent molecules, but also about changes of their fluorescence in time. Dark horizontal stripes and bright semicircles instead of circles represent blinking and bleaching of the molecules in time. Blinking and bleaching are a common, single-molecule phenomenon and convincing evidence of the single-photon nature of the source. The explanation of the nature of the long-time blinking from milliseconds to several seconds remains a subject of debates in the literature, see, e.g., [35].

The maximum count rate of single-molecule images was approximately 10 kcounts/s (~160 counts/pixel with ~4 s per line scan, 256 pixels per line) with a fluorescence lifetime of the molecules approximately several ns. Note that the detector dark counts were fewer than 100 counts/s.

Seven molecules in Figs. 5b and 5c have either positive or zero value of ρ. These molecules could be either a small amount of impurities in photoalignment agent or impurities of the glassy oligomer host [36]. Single-molecule fluorescence microscopy method is very sensitive to the material impurities. Sometimes we observed single-molecule fluorescence from the impurities in glassy liquid-crystal oligomers even when a chromatographic analysis did not show them.

It should be mentioned for comparison that if one calculates the values of ρ from linearly polarized fluorescence data of heterostructured semiconductor QDs in elliptical micropillars and 2-D photonic crystals reported in the literature for cryogenic temperatures [11–15], these values will be between 0.2 and 0.95.

4. CONCLUSIONS

This paper provides simple solution to produce desired circular and linear polarizations of room-temperature single-photon sources—using liquid crystals as the hosts for single fluorescent emitters. Developed polarized single-photon sources can be used as circular and linear polarized basis in a BB84 protocol.

Single semiconductor nanocrystal (colloidal QD) fluorescence in microcavities was studied for the first time. We report the first observation of single-emitter *circularly* polarized fluorescence of definite handedness due to microcavity chirality. The chiral microcavities were prepared by a simple method of planar alignment of *cholesteric* liquid crystals.

Antibunching experiments show that the fluorescence background of the medium is low, so that antibunching of QD fluorescence is preserved.

Single dye molecules were deterministically aligned by *nematic* liquid-crystal molecules in one direction and produced *linearly* polarized single photons with definite polarization.

Our next steps will be increasing the efficiency of our on-demand polarized single-photon sources by selection of emitters with (1) quantum yield ~100% [16], (2) a fluorescence wavelength outside the host fluorescence background, and (3) a fluorescence lifetime shorter than several ns. We also will refine the chiral microcavity preparation technique providing strong coupling between a single emitter and a cavity. Recently we reported on preparation of chiral 1-D photonic bandgap microcavities doped with PbSe QDs with fluorescence maximum at 1.5 μm [8] for a single-photon source at optical telecom wavelengths.

ACKNOWLEDGMENTS

The authors acknowledge the support by the US National Science Foundation (awards ECS-0420888, DUE-063362, and DUE-0920500) and US Army Research Office under Award no. DAAD19-02-1-0285. The authors also thank A.W. Schmid, K. Marshall, L. Novotny, A. Lieb, T. Krauss, M.A. Hahn, C.H. Chen, and J. Dowling. L.J. Bissell thanks the Air Force for a SMART fellowship.

REFERENCES

1. New J. Phys. *Special Issue Focus on Single Photons on Demand*, **6** (2004).
2. P. D. Townsend, Opt. Fiber Technol. **4**, 345 (1998).
3. C. H. Bennett and G. Brassard, in *Proceedings of the IEEE International Conference on Computers, Systems, and Signal Processing* (Bangalor, India, 1984), p. 175.
4. S. G. Lukishova, A. W. Schmid, A. J. McNamar, et al., IEEE J. Selected Topics in Quantum Electronics, Special Issue on Quantum Internet Technologies, **9**, 1512 (2003).

5. S. G. Lukishova, A. W. Schmid, C. M. Supranowitz, N. Lippa, A. J. McNamara, R. W. Boyd, et al., J. Modern Opt. Special Issue on Single Photon, **51** (9–10), 1535 (2004).
6. S. G. Lukishova, A. W. Schmid, R. Knox, P. Freivald, L. J. Bissell, R. W. Boyd, et al., J. Modern Opt. Special Issue on Single Photon, **54** (2–3), 417 (2007).
7. S. G. Lukishova, R. W. Boyd, and C. R. Stroud, US Patent No. 7, 253 871 B2 (Aug. 7, 2007).
8. S. G. Lukishova, L. J. Bissell, V. M. Menon, N. Valappil, M. A. Hahn, C. M. Evans, et al., J. Mod. Opt. Special Issue on Single Photon **56** (2–3), 167 (2009).
9. Y. Yamamoto, C. Santori, J. Vuskovic, et al., Progr. Informat., No. 1, 5 (2005).
10. A. J. Bennett et al., Phys. Stat. Sol. B **243**, (14), 3730 (2006).
11. B. Gayral, J. M. Gerard, B. Legrand, et al., Appl. Phys. Lett. **72**, 1421 (1998).
12. A. Daraei, A. Tahraoui, D. Sanvitto, et al., Appl. Phys. Lett. **88**, 051113 (2006).
13. D. C. Unitt, A. J. Bennett, P. Atkinson, et al., Phys. Rev. B **72**, 033318 (2005).
14. D. Englund, D. Fattal, E. Walks, et al., Phys. Rev. Lett. **95**, 013904 (2005).
15. W.-H. Chang, W.-Y. Chen, H.-S. Chang, et al., Phys. Rev. Lett. **96**, 117401 (2006).
16. J. Yao, D. R. Larson, H. D. Vishwasrao, W. R. Zipfel, and W. W. Webb, Proc. Nat. Acad. Sci. **102** (40), 14284 (2005).
17. H. Huang, A. Dorn, V. Bulovic, and M. Bawendi, Appl. Phys. Lett. **90**, 023110 (2007).
18. Y. Chen, J. Vela, H. Htoon, et al., J. Am. Chem. Soc. **130**, 5026 (2008).
19. H. Shi, B. M. Conger, D. Katsis, and S. H. Chen, Liquid Crystals **24**, 163 (1998).
20. C. B. Murray, D. J. Norris, and M. G. Bawendi, J. Am. Chem. Soc. **115**, 8706 (1993).
21. B. L. Qu, Z. A. Peng, and X. Peng, Nano Lett. **1**, 333 (2001).
22. S. Chanrasekhar, *Liquid Crystals* (Cambridge Univ. Press, Cambridge, 1977).
23. J. P. Dowling, M. Scalora, M. J. Bloemer, and C. M. Bowden, J. Appl. Phys. **75**, 1896 (1994).
24. V. I. Kopp, B. Fan, H. K. M. Vithana, and A. Z. Genack, Opt. Lett. **23**, 1707 (1998).
25. K. Dolgaleva, S. K. H. Wei, S. G. Lukishova, S. H. Chen, K. Schwertz, and R. W. Boyd, J. Opt. Soc. Am. B **25** (9), 1496 (2008).
26. S. H. Chen, D. Katsis, A. W. Schmid, et al., Nature **397**, 506 (1999).
27. C. A. Leatherdale, W.-K. Woo, F. V. Mikulec, and M. G. Bawendi, J. Phys. Chem. B **106**, 7619 (2002).
28. QD absorption cross-section was calculated from the extinction coefficient provided by vendor (Invitrogen). Quantum yield value of QD was also provided by vendor.
29. http://www.witec.de/en/products/snom/alpha300s/alpha300Sflyer. pdf.
30. H. M. P. Chen, D. Katsis, and S. H. Chen, Chem. Mater. **15**, 2534 (2003).
31. I. Chung, K. T. Shimizu, and M. G. Bawendi, Proc. Nat. Acad. Sci. **100**, 405 (2003).
32. We selected the same terminology for ρ as in Ref. [31] to compare our results with random orientation of molecules reported in Ref. [31] for the same dye. In the book by M. Born and E. Wolf *Principles of Optics* (Pergamon, New York, 1998) the ratio $(I_{par} - I_{perp})/(I_{par} + I_{perp})$, is called "degree of polarization."
33. B. Stevens and T. Ha, J. Chem. Phys. **120**, 3030 (2004).
34. J. Y. P. Butter, B. R. Crenshaw, C. Weder, and B. Hecht, Chem. Phys. Chem. **7**, 261 (2006).
35. F. Vargas, O. Hollricher, O. Marti, et al., J. Chem. Phys. **117**, 866 (2002).
36. S. G. Lukishova, A. W. Schmid, R. P. Knox, et al., Mol. Cryst. Liq. Cryst. **454**, 403 (2006).